Tunable and Thermally Stable Luminescence from Polycyclic Aromatic Hydrocarbons Confined in a Zeolitic Imidazolate Framework

Min Tu, Flip de Jong, Cristina Martín, Helge Reinsch, Sabina Rodríguez-Hermida, Arne Meulemans, Eduard Fron, Daniel Escudero, Mark Van der Auweraer, Johan Hofkens, and Rob Ameloot*

Metal–organic frameworks (MOFs) can provide a variety of nanocompartments for the confinement of guest molecules. Furthermore, the emissions of fluorescent molecules can be tuned by confinement. In this study, a solvent-free "bottle-around-ship" method is used to encapsulate perylene and 9,10-dimethylanthracene, two polycyclic aromatic hydrocarbons, in the MOF ZIF-8. Luminescence color tuning is achieved, including white-light emission, when controlling the loading of only a single type of guest. Photophysical analysis suggests that the variations in luminescence result from various guest arrangements in the nanocompartments, as well as host–guest interactions. Because of the tight confinement of the guests, this host–guest system displays excellent luminescence thermal stability.

1. Introduction

Luminescent materials are attractive for application in phosphor-converted white-light-emitting diodes (PC-WLEDs), which feature extensively in our daily lives.[1–3] PC-WLEDs are commonly produced by coating trichromatic red, green, and blue (RGB) phosphors on UV LED chips or yellow phosphors on blue LED chips, based on the principles of chromaticity.[3]

These di- and trichromatic blending strategies may be difficult to implement in the integration process, and can trigger phase separation and color instability during operation.[4–6] Another requirement for PC-WLEDs is the stability against thermal quenching, thereby ensuring efficient light emission at working temperatures of up to 200 °C.[7–9] Recently, single-phase white-light-emitting materials have been proposed as an alternative strategy to pursue fine color-tunability covering the whole visible spectrum and ensuring high luminescence thermal stability.[10–12]

The assembly of inorganic and organic photon-emitting components into metal–organic frameworks (MOFs) can result in versatile platforms for generating luminescent functionalities.[13–18] In addition to the intrinsic luminescence of the metal and/or the linker, the high degree of porosity in MOFs allows the confinement of luminescent guests.[19–23] The luminescence of such host–guest systems can be tuned by engineering the interactions of the guest with the constituents of the MOFs, offering the opportunity to create single-phase white-light emission.[24–33] In addition, the

M. Tu
2020 X-Lab
Shanghai Institute of Microsystem and Information Technology
Chinese Academy of Sciences
Changning Road 865, Shanghai 200050, China

M. Tu, S. Rodríguez-Hermida, R. Ameloot
Centre for Membrane Separations
Adsorption
Catalysis
and Spectroscopy (cMACS)
KU Leuven
Celestijnenlaan 200F, Leuven 3001, Belgium
E-mail: rob.ameloot@kuleuven.be

F. de Jong, C. Martín, E. Fron, M. Van der Auweraer, J. Hofkens
Division of Molecular Imaging and Photonics
Department of Chemistry
KU Leuven
Celestijnenlaan 200F, Leuven 3001, Belgium

H. Reinsch
Institut für Anorganische Chemie
Christian-Albrechts-Universität Kiel
Christian-Albrechts-Platz 4, 24118 Kiel, Germany

A. Meulemans, D. Escudero
Division of Quantum Chemistry and Physical Chemistry
Department of Chemistry
KU Leuven
Celestijnenlaan 200F, Leuven 3001, Belgium

E. Fron, M. Van der Auweraer, J. Hofkens
KU Leuven Core Facility for Advanced Spectroscopy
KU Leuven
Celestijnenlaan 200F, Leuven 3001, Belgium

relatively high thermal stabilities of MOFs would appear to provide the ability to protect confined luminescent guests, thereby enabling consistent luminescence.[23]

The encapsulation of luminescent guests in MOFs has been demonstrated using both postsynthesis loading and the "bottle-around-ship" method (i.e., in-situ loading during framework formation).[34] The former strategy is limited by steric constraints; furthermore, because the guests must be smaller than the MOF pore windows, they might leach out afterward. Although the latter approach allows the encapsulation of guests larger than the MOF pore apertures,[30–33] it is challenging to achieve high loadings through conventional liquid-phase synthesis due to solubility limitations of the guests and competition with solvent molecules.[32] Polycyclic aromatic hydrocarbons (PAHs) are interesting luminescent guests because of their photophysical properties.[35–37] Herein, we report a solvent-free "bottle-around-ship" method for the encapsulation of two PAHs (perylene and 9,10-dimethylanthracene (DMA)) in ZIF-8 (also known as MAF-4),[38,39] a MOF material formed from Zn^{2+} ions and 2-methylimidazolate (mIm) ligands. By controlling the guest loading, we achieved single-phase luminescence color tuning, including white-light emission, as a result of different guest arrangements inside the pores (**Figure 1**). Furthermore, all these host–guest systems displayed high luminescence thermal stability.

2. Results and Discussion

2.1. Solvent-Free Bottle-Around-Ship Encapsulation

ZIF-8 features spherical cavities (diameter: 11.6 Å) interconnected by narrow windows (diameter: 3.4 Å).[38,39] Because of
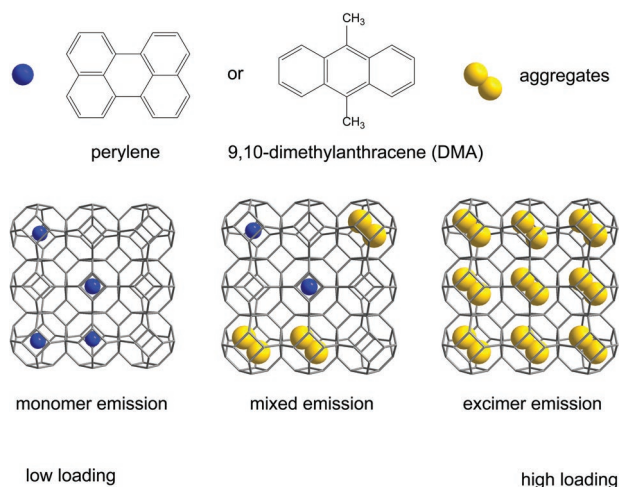

Figure 1. Molecular structures of the emitters perylene and DMA and schematic representation of the luminescence tuning of the PAH@ZIF-8 systems. Solvent-free synthesis enabled tunable loadings of the PAHs confined in the cages of ZIF-8. At low loadings, the PAH molecules were isolated individually in the cages, resulting in their monomer emissions, similar to the luminescence displayed by the molecules in the solution. At high loadings, molecular aggregation occurred in the cages, with the systems exhibiting excimer-like emission. The luminescence could be tuned by varying the relative contributions of the monomer and excimer-like emissions.

the flexibility of the ZIF-8 framework, anthracene can be encapsulated through sublimation, despite its large molecular dimensions (5.6 Å × 9.8 Å).[20] The even bulkier perylene and DMA could not be incorporated using the same strategy. ZIF-8 could be synthesized in a solvent-free manner by heating a solid precursor mixture of zinc oxide (ZnO) and 2-methyl imidazole (HmIm).[40,41] Inspired by that approach, we developed a solvent-free "bottle-around-ship" approach that involves two simultaneous processes: the formation of the MOF framework and the encapsulation (and trapping) of bulky PAHs. The PAH@ZIF-8 host–guest systems were obtained by heating solid mixtures of ZnO, HmIm, and the PAHs. By controlling the PAH contents in the reactant mixtures, we could vary the guest loading from very low to near saturation, as determined using solution ^1H nuclear magnetic resonance (NMR) spectroscopy of acid-digested samples (Figure S1, Supporting Information).

Powder X-ray diffraction (PXRD) patterns of low-loading perylene@ZIF-8 (<2 perylene units/cage) revealed that the 2θ values of all characteristic reflections matched those calculated for ZIF-8 (**Figure 2**a). For the high-loading samples (>2 perylene units/cage), peak splitting of the low-angle reflections [(110), (200), and (211)] occurred, indicating a change in structure relative to that of the guest-free ZIF-8. A Pawley refinement suggested a tetragonal symmetry for ZIF-8 loaded with 2.67 perylene units/cage, different from the cubic symmetry of the guest-free ZIF-8 (Table S1, Supporting Information).[38,39] This analysis also revealed two crystallographically independent cages in which the methyl groups pointed in different directions (Figure 2b and Figure S3, Supporting Information). Nevertheless, Rietveld refinement attempts failed when considering the guests as rigid bodies, likely because of their lack of order or a combination of different ordering geometries. Thermogravimetric analysis (TGA) of perylene@ZIF-8 did not reveal any mass losses prior to the decomposition of the framework (at ≈370°C under an air atmosphere), whereas free perylene starts to sublime near 270 °C (Figure 2d and Figure S6, Supporting Information). This finding implies tight confinement of the guest molecules within the pores. According to the TGA residual and the perylene loading, the ZnO–to–ZIF-8 conversion was almost complete (>99%, Supporting Information Section S3.8). The Brunauer–Emmett–Teller (BET) surface areas of the perylene@ZIF-8 systems decreased gradually upon increasing the guest loading (Figure 2c and Figure S7, Supporting Information). We conclude that variable loadings of perylene, from very low to nearly saturated, could be encapsulated inside the ZIF cages when using this solvent-free "bottle-around-ship" strategy. Similarly, we used the same process to encapsulate DMA with variable loadings (Figures S8–S11, Supporting Information).

2.2. Tunable Luminescence of PAHs@ZIF-8

Figure 3a presents the fluorescence emission spectra of perylene@ZIF-8 at various loadings. Monomeric emission occurred for the low-loading sample (0.04 perylene units/cage), similar to that from dilute perylene solutions (Figure S12, Supporting Information).[42] This behavior suggests that individual perylene molecules were isolated in these ZIF-8 cages. The
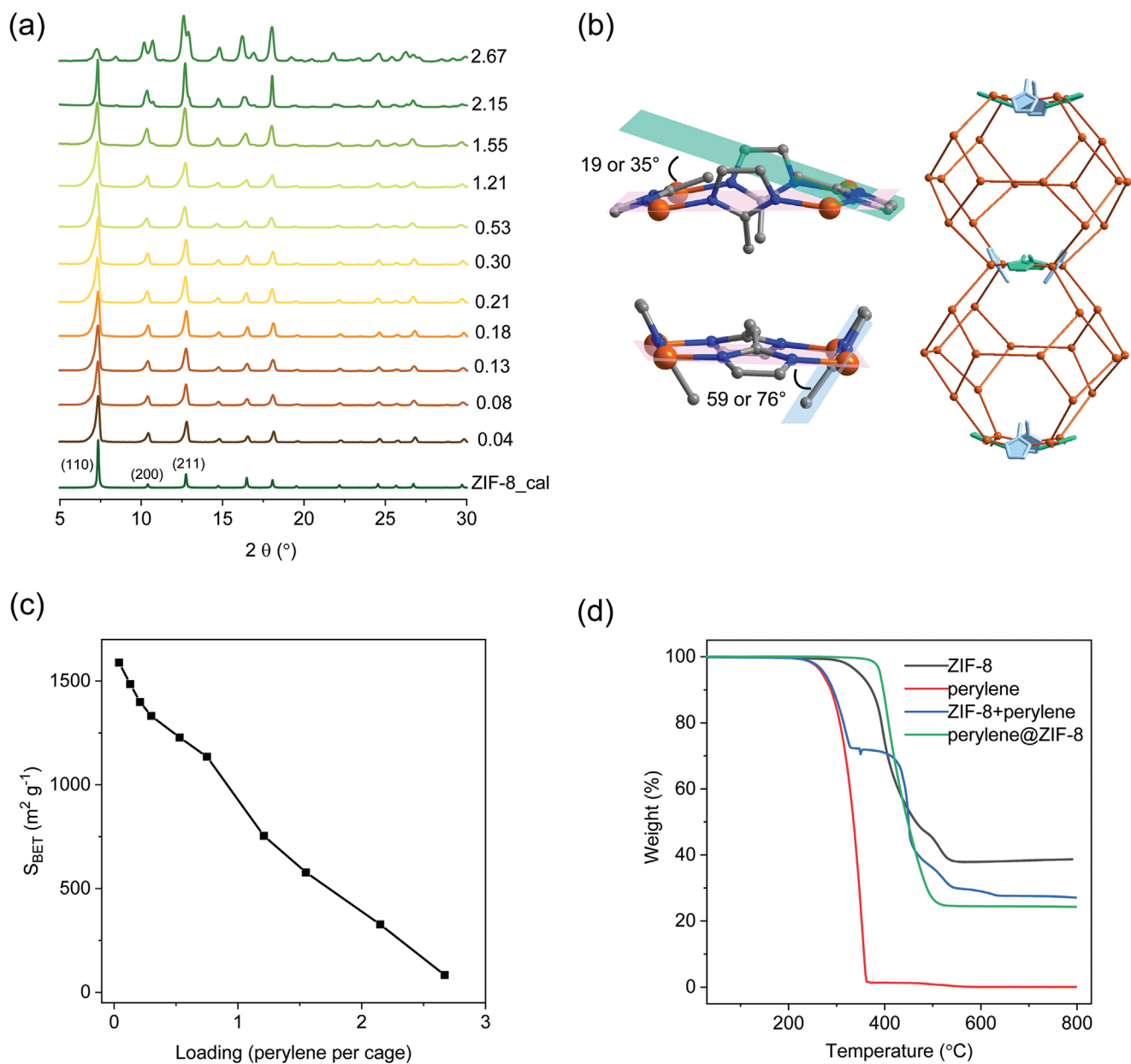
Figure 2. Characterization of perylene@ZIF-8. a) PXRD patterns of perylene@ZIF-8 systems with different loadings (perylene units/cage). b) Illustration of the opening angles between the planes defined by the imidazole rings and by the Zn atoms for perylene@ZIF-8 (2.67 units/cage). There are two types of four-membered-ring windows: one having opening angles of 19° and 35°, and another having opening angles of 59° and 76°. c) BET surface area plotted with respect to the perylene loading. d) TGA of ZIF-8, perylene, a ZIF-8 + perylene physical mixture (≈30 wt%), and perylene@ZIF-8 (2.67 units/cage), measured under an air atmosphere.

Commission International de I'Eclairage (CIE) coordinates (Figure 3b) of perylene@ZIF-8 (0.04 units/cage) were (0.14, 0.19), appearing as a greenish-blue emission. At high loadings (>0.53 units/cage), the fluorescence (λ_{max} = 650 nm) was that of a structureless excimer-like emission.[36,43] The CIE coordinates (Figure 3b) for perylene@ZIF-8 at the highest loading (2.67 units/cage) were (0.60, 0.40), close to those (0.66, 0.33) for a saturated red emitter. When the loading was between 0.04 and 0.53 perylene units/cage, the ratio of monomer and excimer-like emissions changed dramatically, thereby resulting in fluorescence varying from greenish-blue to reddish-orange

(Figure 3b). The fluorescence of perylene@ZIF-8 (0.21 units/cage) covered almost the entire visible spectrum (430–800 nm), resulting in CIE coordinates of (0.29, 0.34), close to those of ideal white light (0.33, 0.33). The correlated color temperature (CCT) was 6570 K, corresponding to the "daylight" color temperature The color-rendering index (CRI) of 87 for this material suggests a suitability for indoor illumination.[6] Single-phase white-light emission has been reported previously for a guest@MOF system, but the strategy required the simultaneous loading of red-, green-, and blue-emitting components in a single MOF.[32] In this study, however, we achieved ready
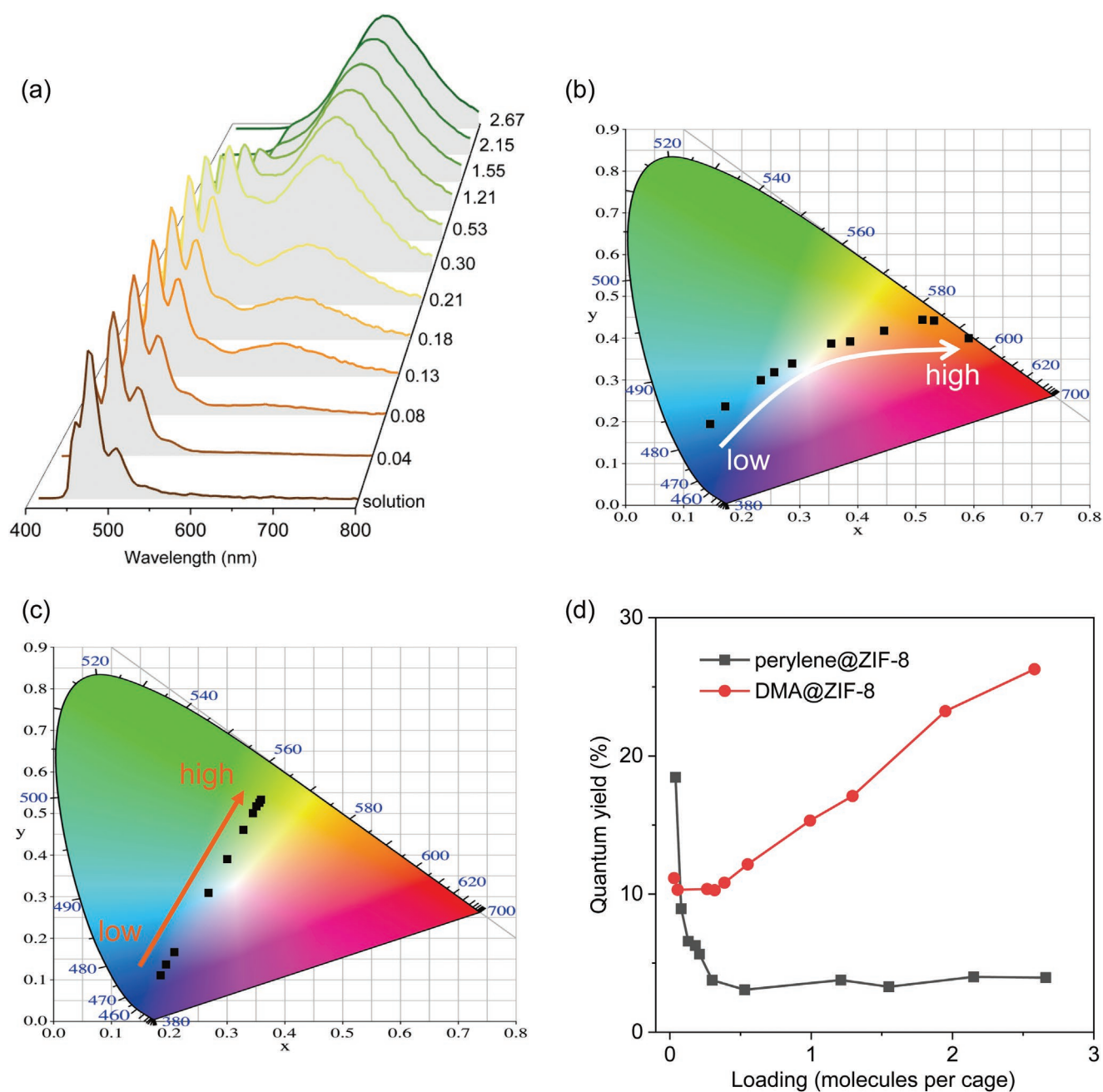
Figure 3. Photoluminescence properties of PAHs@ZIF-8. a) Fluorescence emission spectra of perylene@ZIF-8 with different loadings (units/cage), excited at 390 nm. The spectrum of perylene in solution (0.1 mM in DMF) is given as a reference. b,c) CIE coordinates of (b) perylene@ZIF-8 and (c) DMA@ZIF-8 at various PAH loadings. The spectra of DMA@ZIF-8 are presented in Figure 4a and Figures S15 and S16 (Supporting Information). d) PLQYs of perylene@ZIF-8 and DMA@ZIF-8 plotted with respect to the PAH loading (units/cage); excitation wavelengths for perylene@ZIF-8 and DMA@ZIF-8: 390 and 380 nm, respectively.

luminescence tuning, including white-light emission, through variable loading of only a single type of guest.

We also achieved tunable fluorescence upon controlling the loading of DMA in ZIF-8 (Figures 3c and 4a). The fluorescence emission of DMA@ZIF-8 (0.03 units/cage) was characteristic of monomer emission (Figure S15, Supporting Information) with CIE coordinates of (0.17, 0.09), close to those of a saturated blue emitter (0.14, 0.08).[44] The highest loading of DMA

(2.58 units/cage) resulted in a greenish-yellow emission with CIE coordinates of (0.36, 0.56), corresponding to an excimer-like emission (vide infra). Similar to perylene@ZIF-8, the fluorescence of DMA@ZIF-8 was tunable for loadings between 0.03 and 0.55 units/cage. Furthermore, white-light emission resulted from a combination of blue and yellow emissions. At a loading of 0.32 units/cage, the CIE coordinates were (0.28, 031) close to those for ideal white light (0.33, 0.33).
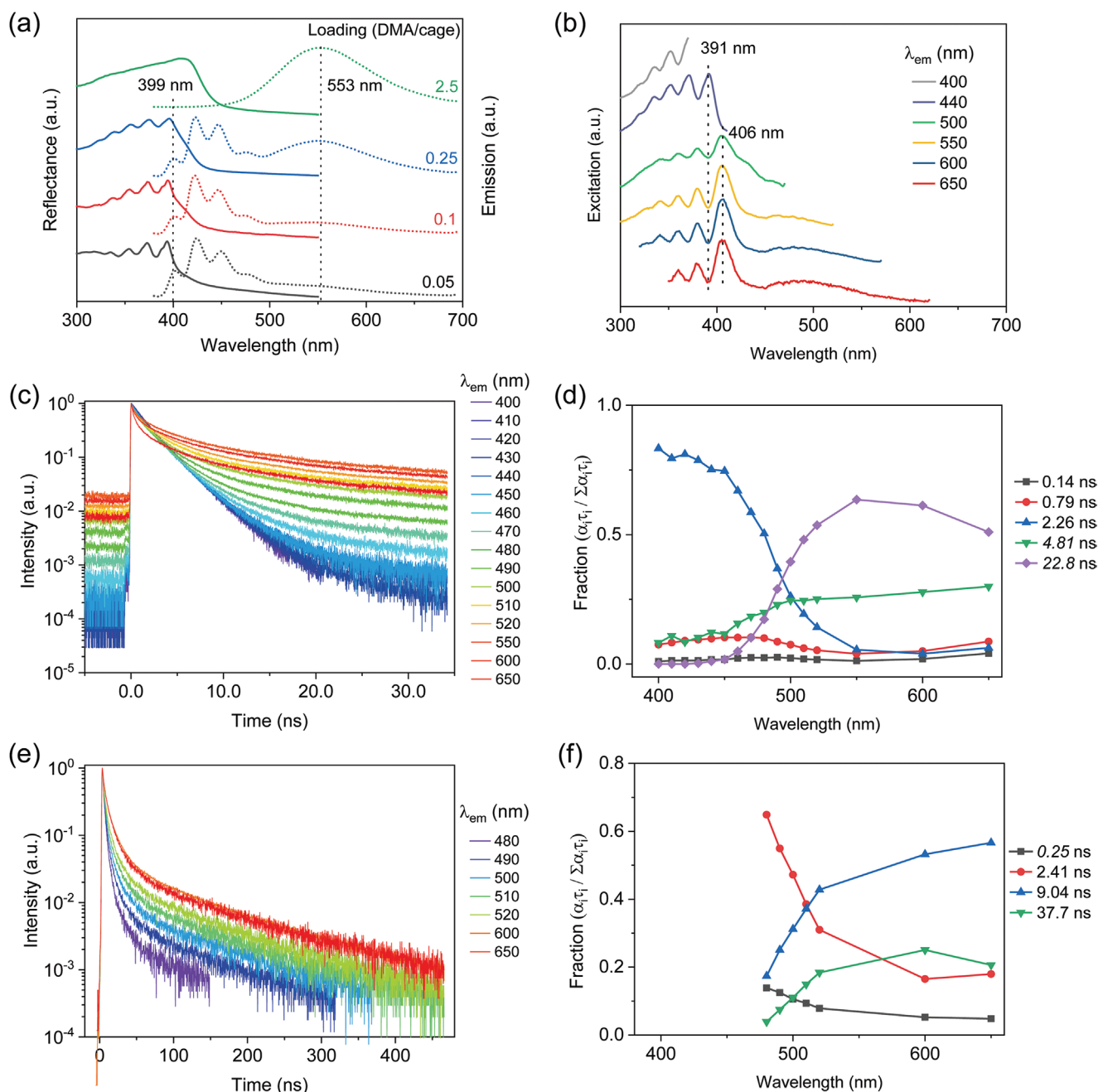
Figure 4. Photoluminescence of DMA@ZIF-8. a) Steady-state diffuse reflectance (solid line) and emission (dashed line) spectra (λ_{exc} = 350 nm) recorded at various loadings. b) Steady-state excitation spectra of DMA@ZIF-8 (0.10) recorded at various emission wavelengths. c) Normalized fluorescence decays (λ_{exc} = 375 nm) of DMA@ZIF-8 (0.10 units/cage) measured at various emission wavelengths in tens of nanoseconds window and d) the parameters recovered through analysis of the decays as a sum of exponentials. e) Normalized fluorescence decays (λ_{exc} = 375 nm) of DMA@ZIF-8 (0.10 units/cage) measured at various emission wavelengths in hundreds of nanoseconds window and f) the parameters recovered through analysis of the decays as a sum of exponentials. Decay times in italics are not accurate in the respective time regimes.

The photoluminescence quantum yield (PLQY) is an important characteristic for the application of any luminescent phosphor. For perylene@ZIF-8, increasing the loading of perylene decreased the PLQY significantly, from 18% to ≈3%. At low loadings, perylene molecules were trapped individually in the cages, whereas aggregates formed at high loadings, resulting in significant decreases in the PLQYs. Interestingly, the PLQYs of DMA@ZIF-8 exhibited the opposite trend: the PLQY increased from 10% at low loadings to ≈28% at high loadings (Figure 3d). The PLQYs of the perylene monomer and excimer in deoxygenated benzene are 82% and 2%, respectively,[42] whereas the PLQYs of the DMA monomer and excimer fluorescence in deoxygenated benzene are 75% and 24%, respectively.[45] While the PLQYs of the encapsulated excimer were

close to those of the corresponding excimers in solution, the PLQYs of the encapsulated monomers were four to seven times lower than in solution. We suspect that this difference is due to more efficient quenching of the monomer by energy transfer to low-lying states in ZIF-8 compared with the excimer excited states (see additional discussion in the Supporting Information Section S5).

2.3. Fluorescence of DMA@ZIF-8

The steady-state emission spectra of DMA@ZIF-8 (Figure 4a) suggested the presence of a monomer providing a structured emission with a 0–0 transition at 399 nm and an excimer-like emission, initially appearing as a red tail, with a maximum close to 553 nm. The relative importance of the latter emission increased at high loadings [see the two-dimensional (2D) spectra in Figures S15 and S16, Supporting Information]. In the excitation spectra of DMA@ZIF-8 (0.1) (Figure 4b), we observe three systems: 1) a structured band centered around 391 nm, predominant for the monomer emission; 2) a structured band having a maximum at 406 nm; and 3) a weak broad band centered around 480 nm. The diffuse reflectance spectra (Figure 4a) can be considered a superposition of the monomer and dimer excitation spectra, with the monomer being the dominant species at the lower loadings. The bands of maximum intensity at 391 nm in the excitation spectra and at 398 nm for the 0–0 transition in the emission spectra agree with the emission and absorption spectra obtained by Wolff et al. for DMA monomers in cyclodextrin.[44] Because the excimer-like emission (553 nm) appeared at a significantly longer wavelength than those of the stable dimer of anthracene,[46] the crystal spectrum of dimethyllanthracene,[44] and the partial-overlap excimer of anthracene,[47] we suspect that the geometry of the emitting species was close to that of the sandwich excimer. The excimer-like emission was blueshifted relative to the emission of the solution excimer of DMA (571 nm), presumably because the MOF framework induced deviations from the perfect sandwich geometry.[45] The absorption of a ground-state sandwich dimer would be blueshifted rather than redshifted,[46] while a red-shifted structured absorption band has been observed for the stable dimer of anthracene and for dimers of chloroanthracene in an organic glass after softening.[46] This suggests that dimers having a different geometry in the ground state relaxed toward a sandwich configuration after excitation.

We used time-correlated single-photon counting (TC-SPC) to measure the fluorescence decays in two different time windows: tens of nanoseconds and hundreds of nanoseconds (Figure 4c,e). The long-lived excimer emission accumulated over several pulses in the shorter-timescale experiment, distorting the longer lifetimes. Global multiexponential analysis of decays obtained at different wavelengths required at least five decay times (Figure 4d,f). This prerequisite suggested a very complex decay, implying that the individual decay times had limited physical meaning. Figure 4c plots the wavelength-dependence of the fractional contribution of each recovered lifetime for DMA@ZIF-8 (0.10 units/cage). The main component in the blue part of the spectrum had a lifetime of 2.26 ns, considerably shorter than those reported previously (>7 ns for

air-saturated solutions of DMA).[44] This lifetime is consistent with the lower quantum yield of fluorescence ($\approx$10%; cf. 75% in solution) and resulted from increased nonradiative decay or quenching of the emission of the DMA monomers by the ZIF-8 framework.[45] The major components for the excimer-like emission had decay times of 9.04 and 37.7 ns (Figure 4f). These decay times are significantly shorter than that reported for the DMA excimer (220 ns),[48] possibly due to O_2-mediated quenching of the emission (samples had not been deoxygenated), and/or from perturbation of the perfect sandwich geometry induced by the ZIF-8 framework. The latter would make the radiative transition from the lowest exciton state to the ground state partially allowed, and it is consistent with the broadband centered around 480 nm in the excitation spectrum. Although the data could be analyzed in terms of a multiexponential decay, it is more likely that the distribution of aggregate geometries, or different interactions with the framework, led to a continuous distribution of decay times. Combining the quantum yield of $\approx$30% at high loading with the decay times on the order of 10–40 ns, we obtained radiative rate constants ranging from 3×10^7 to 7.5×10^6 s^{-1} for the excimer emission. These values are higher than that of the DMA excimer (4.5×10^6 s^{-1}). Again, this finding suggests that deviations from the perfect sandwich geometry led to similar increases in the rate constants for the radiative and nonradiative decay processes.

A computational study was performed to substantiate the conclusions of the photophysical study. For ZIF-8 with one DMA molecule per cage, only one local minimum was found in the ground state (S_0), with an interaction energy of –43.9 kcal mol^{-1}. When modeling two DMA molecules in the ZIF-8 cavity in S_0, four different local minima were obtained (Figure S25 and Table S3, Supporting Information): i) a minimum where the two DMA molecules interact solely with the MOF and not with each other, ii) a sandwich π-stacked minimum, iii) a staggered π-stacked minimum, and iv) a diagonal T-shape π-stacked minimum, in which one of the DMA molecules also partially interacts with ZIF-8. The calculations show that the staggered π-stacked minimum (**Figure 5**a) is the most favorable conformer in the ground state, followed by the sandwich π-stacked and the diagonal T-shape π-stacked minima. The favorable nature of the sandwich π-stacked minimum compared with two separate DMA molecules could explain the observation of significant excimer emission even at low loadings (Figure 4a). This sandwich π-stacked minimum will be populated to some extent in the ground state, resulting in the broad structureless band around 500 nm in the excitation spectra (Figure 4b).

The first excited state (S_1) potential energy surface (PES) for the binary and ternary complexes was also explored. For the excited states of the ternary complexes, the optimizations started from the two most stable conformers only, i.e., the sandwich π-stacked minimum and the staggered π-stacked minimum, and yielded minima with similar topology to those found in S_0 (Figure S26, Supporting Information). In contrast with the results in the S_0 PES, in the S_1 PES, the most stable conformer is the sandwich π-stacked minimum (Figure 5b), which is favored by 6.6 kcal mol^{-1} (Table S4, Supporting Information). Interestingly, the centroid-to-centroid distance in the sandwich π-stacked conformation decreases when going from
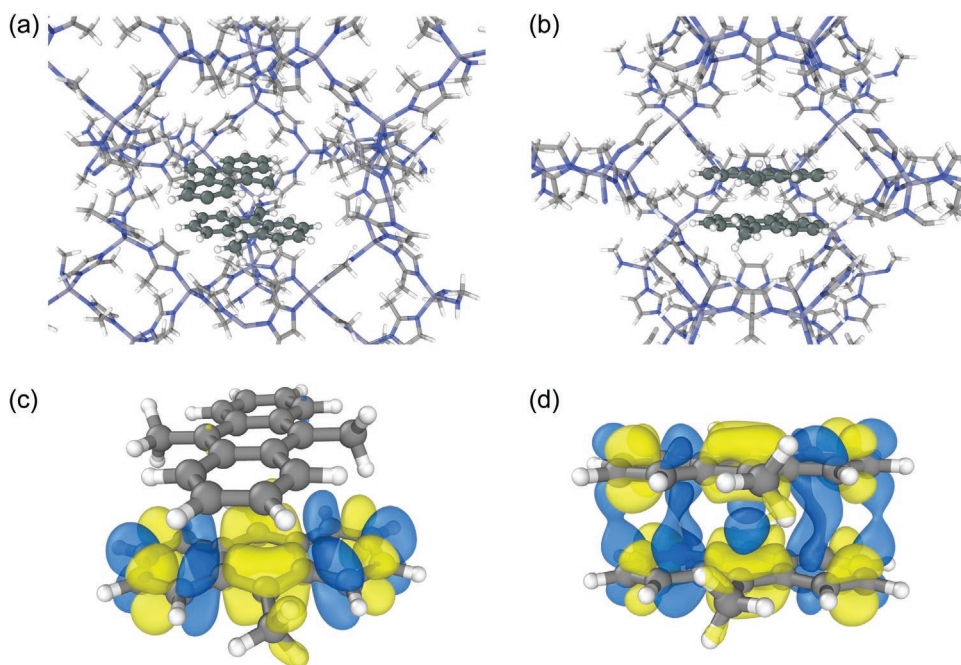
Figure 5. Computational results for DMA@ZIF-8. a) Optimized geometry of the staggered π-stacked minimum in the ground state (S_0). b) Optimized geometry of the sandwich π-stacked minimum in the lowest singlet excited state (S_1). c) S_1 electron density difference (EDD) plot for the staggered π-stacked conformer at its optimized S_0 geometry. Blue (yellow) regions represent increase (depletion) of electron density in S_1. d) S_1 electron density difference (EDD) plot for the sandwich π-stacked conformer at its optimized S_1 geometry. Blue (yellow) regions represent increase (depletion) of electron density in S_1.

the S_0 to the S_1 scenario (3.89–3.36 Å in Table S4, Supporting Information), a clear indication of the formation of excimers. The character of S_1 notably changes from a predominantly local excited state at the S0 geometry (see the electron density difference (EDD) plot in Figure 5c) to a predominantly excimer-like excited state at the optimized S_1 geometry (Figure 5d), where the electron density is fully delocalized within the two DMA moieties. The calculated emission energies can be found in Table S4 (Supporting Information). The computed emission energy for ZIF-8 with one DMA molecule inside the cage is 416 nm, which is in good agreement with the monomer-like emission observed experimentally (391 nm). The experimentally determined peak excimer emission (553 nm) agrees better with the calculated emission from the sandwich π-stacked ternary complex (574 nm) than from the staggered π-stacked conformer (449 nm). These results corroborate the results discussed above for the ternary complexes, as well as the conclusions from the photophysical study.

2.4. Thermally Stable Luminescence

The generation of heat during LED operation typically leads to pronounced emission losses that seriously affect the efficiency and alter the white balance of the white-light emission.[8] Thus, high thermal stability is required for any luminescent materials used in PC-WLEDs. In our present host–guest systems, physical trapping of the PAHs in the cages of ZIF-8 prevented leakage of the guest molecules from the frameworks, even at high temperatures (up to the decomposition temperature of the framework). TGA profiles revealed that no mass losses

occurred when the host–guest systems were kept isothermal for 2 h, exposed to the air, or at multiple temperatures in the range of 150–250 °C (**Figure 6**a), demonstrating their excellent thermal stability. The fluorescence emission spectra of perylene@ZIF-8 (0.21 units/cage) at 150 and 200 °C were similar to that recorded at room temperature, albeit with slightly increased intensities (Figure S28, Supporting Information). The fluorescence emission spectra of perylene@ZIF-8 (0.21) at an isothermal trajectory at 150 and 200 °C for 5 h of exposure to the air exhibited negligible spectral shifts or intensity changes for either the monomer or excimer emission, implying the absence of molecular mobility between the cages (Figure 6b–d). These results confirm the high luminescence thermal stabilities of these host–guest systems (Figures S29–S32, Supporting Information).

3. Conclusion

A "bottle-around-ship" encapsulation strategy makes it possible to control the loadings of PAH molecules in ZIF-8, resulting in single-phase luminescence tuning and white-light emission when only one type of guest is present. The tuning of the luminescence resulted from the different states of organization of the PAH molecules within the MOF cavities. The PAH@ZIF-8 systems displayed high luminescence thermal stability, resulting from the tight confinement of the PAHs in the ZIF-8 cages. Our study suggests that confinement of luminescent guests in porous MOFs is a promising strategy for luminescence tuning, with potential for applications in solid-state lighting.
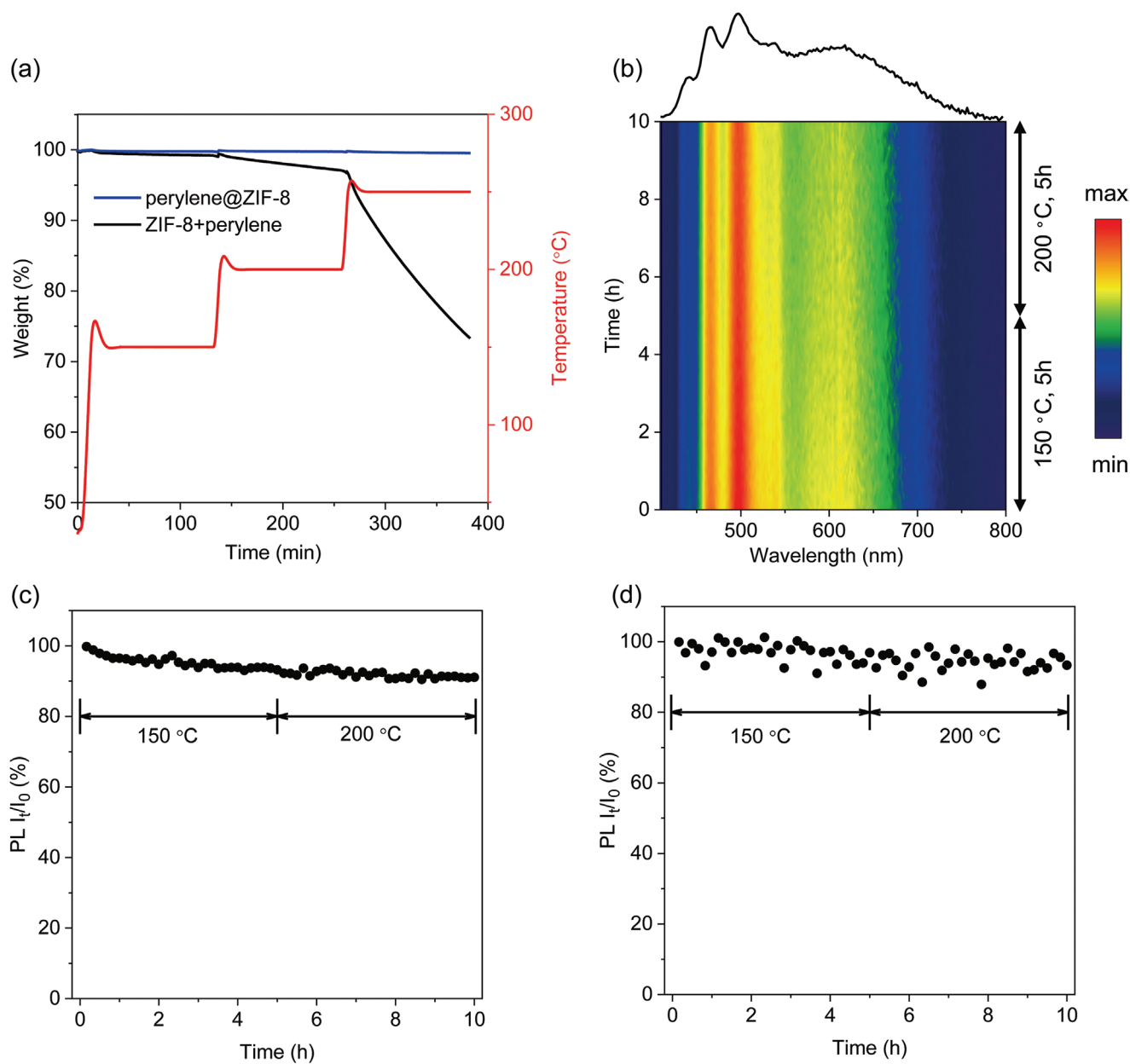
Figure 6. Thermal stability of perylene@ZIF-8. a) TGA of perylene@ZIF-8 (2.67 units/cage) and a ZIF-8 + perylene physical mixture (≈30 wt%) after isothermal treatment at temperatures of 150, 200, and 250 °C for 2 h. b) Fluorescence emission spectra of perylene@ZIF-8 (0.21 units/cage) measured at 150 and 200 °C in an air atmosphere, recorded every 10 min. c,d) Changes in the fluorescence emission intensity (I_t/I_0) at (c) 500 and (d) 630 nm, plotted with respect to time, measured at 150 and 200 °C.

Keywords

[1] C. Feldmann, T. Jüstel, C. R. Ronda, P. J. Schmidt, *Adv. Funct. Mater.* **2003**, *13*, 511.

[2] K. T. Kamtekar, A. P. Monkman, M. R. Bryce, *Adv. Mater.* **2010**, *22*, 572.

[3] S. Ye, F. Xiao, Y. X. Pan, Y. Y. Ma, Q. Y. Zhang, *Mater. Sci. Eng. R Rep.* **2010**, *71*, 1.

[4] X. Gong, S. Wang, D. Moses, G. C. Bazan, A. J. Heeger, *Adv. Mater.* **2005**, *17*, 2053.

[5] W. Baekelant, E. Coutino-Gonzalez, J. A. Steele, M. B. J. Roeffaers, J. Hofkens, *ACS Energy Lett.* **2017**, *2*, 2491.

[6] Y. Tang, H. Wu, W. Cao, Y. Cui, G. Qian, *Adv. Opt. Mater.* **2021**, *9*, 2001817.

[7] Y. Zhao, C. Riemersma, F. Pietra, R. Koole, C. de Mello Donegá, A. Meijerink, *ACS Nano* **2012**, *6*, 9058.

[8] Y. H. Kim, P. Arunkumar, B. Y. Kim, S. Unithrattil, E. Kim, S.-H. Moon, J. Y. Hyun, K. H. Kim, D. Lee, J.-S. Lee, W. B. Im, *Nat. Mater.* **2017**, *16*, 543.

[9] Y.-C. Lin, M. Bettinelli, M. Karlsson, *Chem. Mater.* **2019**, *31*, 3851.

[10] M. Shang, C. Li, J. Lin, *Chem. Soc. Rev.* **2014**, *43*, 1372.

[11] Q.-W. Zhang, D. Li, X. Li, P. B. White, J. Mecinović, X. Ma, H. Ågren, R. J. M. Nolte, H. Tian, *J. Am. Chem. Soc.* **2016**, *138*, 13541.

[12] S. A. Khan, N. Z. Khan, M. Sohail, J. Ahmed, N. Alhokbany, S. M. Alshehri, X. Xu, J. Zhu, S. Agathopoulos, *J. Mater. Chem. C* **2021**, *9*, 13041.

[13] Y. Cui, Y. Yue, G. Qian, B. Chen, *Chem. Rev.* **2012**, *112*, 1126.

[14] K. Müller-Buschbaum, F. Beuerle, C. Feldmann, *Microporous Mesoporous Mater.* **2015**, *216*, 171.

[15] W. P. Lustig, S. Mukherjee, N. D. Rudd, A. V. Desai, J. Li, S. K. Ghosh, *Chem. Soc. Rev.* **2017**, *46*, 3242.

[16] Y. Cui, J. Zhang, H. He, G. Qian, *Chem. Soc. Rev.* **2018**, *47*, 5740.

[17] M. Pan, W.-M. Liao, S.-Y. Yin, S.-S. Sun, C.-Y. Su, *Chem. Rev.* **2018**, *118*, 8889.

[18] H.-Q. Yin, X.-B. Yin, *Acc. Chem. Res.* **2020**, *53*, 485.

[19] H. He, Y. Cui, B. Li, B. Wang, C. Jin, J. Yu, L. Yao, Y. Yang, B. Chen, G. Qian, *Adv. Mater.* **2019**, *31*, 1806897.

[20] M. Tu, H. Reinsch, S. Rodríguez-Hermida, R. Verbeke, T. Stassin, W. Egger, M. Dickmann, B. Dieu, J. Hofkens, I. F. J. Vankelecom, N. Stock, R. Ameloot, *Angew. Chem., Int. Ed.* **2019**, *58*, 2423.

[21] Y. Shu, Q. Ye, T. Dai, Q. Xu, X. Hu, *ACS Sens.* **2021**, *6*, 641.

[22] G. A. Leith, C. R. Martin, J. M. Mayers, P. Kittikhunnatham, R. W. Larsen, N. B. Shustova, *Chem. Soc. Rev.* **2021**, *50*, 4382.

[23] M. Gutiérrez, Y. Zhang, J.-C. Tan, *Chem. Rev.* **2022**, *11*, 10438.

[24] Y. Cui, T. Song, J. Yu, Y. Yang, Z. Wang, G. Qian, *Adv. Funct. Mater.* **2015**, *25*, 4796.

[25] W. Xie, W.-W. He, D.-Y. Du, S.-L. Li, J.-S. Qin, Z.-M. Su, C.-Y. Sun, Y.-Q. Lan, *Chem. Commun.* **2016**, *52*, 3288.

[26] Y. Wen, T. Sheng, X. Zhu, C. Zhuo, S. Su, H. Li, S. Hu, Q.-L. Zhu, X. Wu, *Adv. Mater.* **2017**, *29*, 1700778.

[27] W. Chen, Y. Zhuang, L. Wang, Y. Lv, J. Liu, T.-L. Zhou, R.-J. Xie, *ACS Appl. Mater. Interfaces* **2018**, *10*, 18910.

[28] Y. Tang, T. Xia, T. Song, Y. Cui, Y. Yang, G. Qian, *Adv. Opt. Mater.* **2018**, *6*, 1800968.

[29] H. Li, Q. Li, Z. Xu, *J. Mater. Chem. C* **2019**, *7*, 2880.

[30] Y. Chen, B. Yu, Y. Cui, S. Xu, J. Gong, *Chem. Mater.* **2019**, *31*, 1289.

[31] X.-Y. Liu, Y. Li, C.-K. Tsung, J. Li, *Chem. Commun.* **2019**, *55*, 10669.

[32] X.-Y. Liu, K. Xing, Y. Li, C.-K. Tsung, J. Li, *J. Am. Chem. Soc.* **2019**, *141*, 14807.

[33] T. Xiong, Y. Zhang, L. Donà, M. Gutiérrez, A. F. Möslein, A. S. Babal, N. Amin, B. Civalleri, J.-C. Tan, *ACS Appl. Nano Mater.* **2021**, *4*, 10321.

[34] U. Ryu, H. S. Lee, K. S. Park, K. M. Choi, *Polyhedron* **2018**, *154*, 275.

[35] T. H. Noh, H. Lee, J. Jang, O.-S. Jung, *Angew. Chem., Int. Ed.* **2015**, *54*, 9284.

[36] R. Katoh, K. Suzuki, A. Furube, M. Kotani, K. Tokumaru, *J. Phys. Chem. C* **2009**, *113*, 2961.

[37] W. E. A. jr , S. A. Tucker, J. C. Fetzer, *Polycycl. Aromat. Compd.* **2006**, *2*, 75.

[38] K. S. Park, Z. Ni, A. P. Côté, J. Y. Choi, R. Huang, F. J. Uribe-Romo, H. K. Chae, M. O'Keeffe, O. M. Yaghi, *Proc. Natl. Acad. Sci. U.S.A.* **2006**, *103*, 10186.

[39] X.-C. Huang, Y.-Y. Lin, J.-P. Zhang, X.-M. Chen, *Angew. Chem., Int. Ed.* **2006**, *45*, 1557.

[40] I. Stassen, M. Styles, G. Grenci, H. V. Gorp, W. Vanderlinden, S. D. Feyter, P. Falcaro, D. D. Vos, P. Vereecken, R. Ameloot, *Nat. Mater.* **2016**, *15*, 304.

[41] T. Stassin, I. Stassen, J. Marreiros, A. J. Cruz, R. Verbeke, M. Tu, H. Reinsch, M. Dickmann, W. Egger, I. F. J. Vankelecom, D. E. De Vos, R. Ameloot, *Chem. Mater.* **2020**, *32*, 1784.

[42] R. Katoh, S. Sinha, S. Murata, M. Tachiya, *J. Photochem. Photobiol. Chem.* **2001**, *145*, 23.

[43] H. Auweter, D. Ramer, B. Kunze, H. C. Wolf, *Chem. Phys. Lett.* **1982**, *85*, 325.

[44] T. Wolff, K. Pfanner, C. Springob, *J. Photochem. Photobiol. Chem.* **1993**, *74*, 247.

[45] BarnesR. L. , BirksJ. B. , F. B. Hilton, *Proc. R. Soc. Lond. Ser. Math. Phys. Sci.* **1966**, *291*, 570.

[46] E. A. Chandross, J. Ferguson, E. G. McRae, *J. Chem. Phys.* **1966**, *45*, 3546.

[47] C. Zhao, X. Cai, Z. Ma, J. Shi, L. Xu, H. Wang, *J. Photochem. Photobiol. Chem.* **2018**, *355*, 318.

[48] J. Birks, *Photophysics of Aromatic Molecules*, Wiley-Interscience, London **1970**.